

Associated Spectral and Temporal State Transition of the bright ULX NGC 1313 X-1

G. C. Dewangan^{1*}, R. Misra^{1†}, A. R. Rao^{2‡} and R. E. Griffiths^{3§}

¹*IUCAA, Post Bag 4, Ganeshkhind, Pune 411 007, India*

²*Department of Astronomy & Astrophysics, Tata Institute of Fundamental Research, Homi Bhabha Road, Mumbai, 400005 India*

³*Department of Physics, Carnegie Mellon University, 5000 Forbes Avenue, Pittsburgh, PA 15213 USA*

Accepted for publication in MNRAS

ABSTRACT

Stellar mass black hole X-ray binaries exhibit X-ray spectral states which also have distinct and characteristic temporal properties. These states are believed to correspond to different accretion disc geometries. We present analysis of two *XMM-Newton* observations of the Ultra-Luminous X-ray source (ULX) NGC 1313 X-1, which reveal that the system was in two different spectral states. While spectral variations have been observed in this source before, this data provides clear evidence that the spectral states also have distinct temporal properties. With a count rate of ~ 1.5 counts/s and a fractional variability amplitude of $\sim 15\%$, the ULX was in a high flux and strongly variable state in March 2006. In October 2006, the count rate of the ULX had reduced by a factor of ~ 2 and the spectral shape was distinctly different with the presence of a soft component. No strong variability was detected during this low flux state with an upper limit on the amplitude $< 3\%$. Moreover, the spectral properties of the two states implies that the accretion disc geometry was different for them. The low flux state is consistent with a model where a standard accretion disc is truncated at a radius of ~ 17 Schwarzschild radius around a $\sim 200M_{\odot}$ black hole. The inner hot region Comptonizes photons from the outer disc to give the primary spectral component. The spectrum of the high flux state is not compatible with such a geometry. Instead, it is consistent with a model where a hot corona covers a cold accretion disc and Comptonizes the disc photons. The variability as a function of energy is also shown to be consistent with the corona model. Despite these broad analogies with Galactic black hole systems, the spectral nature of the ULX is distinct in having a lower temperature (~ 2 keV) of the hot Comptonizing plasma and higher optical depth (~ 15) than what is observed for the Galactic ones.

Key words: Accretion, Accretion Discs, Black Hole Physics, X-Rays: Binaries, X-Rays: Galaxies, X-rays: individual: NGC 1313 X-1

1 INTRODUCTION

Ultra-luminous X-ray sources (ULXs) are off-nuclear, compact X-ray sources with luminosities exceeding $\sim 10^{39}$ erg s⁻¹. The nature of ULXs continues to be an enigma, since their isotropic high energy output surpasses the Eddington limit of even the most massive stellar mass black holes, sometimes by large factors. One individual ULX may outshine the rest of the galaxy in the high energy X-ray band. Several models have been proposed to explain the high luminosities of ULXs. They may be powered by “in-

termediate mass black hole (IMBH)” with masses $M_{BH} \simeq 10^2 - 10^4 M_{\odot}$ (e.g., Colbert & Miller 2005) which bridge the gap between stellar mass black holes in X-ray binaries (XRBs) and super-massive black holes in active galactic nuclei. On the other hand, they may be XRBs with anisotropic emission (King et al. 2001) or beamed XRBs with relativistic jets directly pointing towards us, i.e., scaled down versions of blazars (Mirabel & Rodríguez 1999). Alternatively, they may be stellar mass black holes with super-Eddington accretion rates (Begelman 2002; Poutanen et al. 2007; King 2008).

In the absence of a direct measurement of the black hole mass in ULX, indirect evidence is provided by the spectral and temporal properties of these sources. Qualitative and quantitative similarities (and differences) between them and

* gulabd@iucaa.ernet.in

† rmisra@iucaa.ernet.in

‡ arrao@tifr.res.in

§ griffith@seren.phys.cmu.edu

Galactic X-ray binaries harbouring stellar mass black holes can provide insight into their nature. The discovery of orbital modulations from the bright ULX M 82 X-1 (Kaaret et al. 2006; Kaaret & Feng 2007) and possibly from a ULX in IC 342 (Sugiho et al. 2001) implies that they too are binary systems.

Galactic X-ray binaries exhibit spectral states (e.g. see Zdziarski & Gierliński 2004, for a review). Detailed spectral modelling of these systems reveal that the accretion discs have different geometries for different states. In the high soft state, the spectra are dominated by emission from a cold accretion disc which extends probably to the inner most stable orbit. A corona or active region above the cold disc Comptonizes disc photons to produce hard X-rays. In the low/hard state, the disc is truncated at a larger radius and the X-rays originate from a hot inner region. In the very high state, the geometry is probably similar to that of the high state, but here the flux from the corona is nearly equal to that of the disc. X-ray binaries are variable on a wide range of time-scales and exhibit broad band noise as well as narrow features called Quasi-periodic oscillations (QPO). Spectral state transitions are always associated with distinct changes in the rapid temporal behaviour of the systems.

Both *Chandra* and *XMM-Newton* observations of ULXs have sometimes shown soft X-ray excess emission which has been interpreted as the optically thick emission from thin accretion discs with temperatures in the range of $\sim 100 - 300$ eV, which indicates that they are IMBH accreting at sub-Eddington ($\sim 0.1L_{Edd}$) rates (e.g., Miller et al. 2003; Kaaret et al. 2003; Miller et al. 2004). While this suggests that ULX may be scaled up versions of X-ray binaries, it should be noted that there are important spectral differences. Unlike X-ray binaries, a high energy spectral curvature has been detected in the high quality X-ray spectra of a number of bright ULXs (Agrawal & Misra 2006; Stobbart et al. 2006; Goad et al. 2006; Dewangan et al. 2006; Roberts 2007). This spectral curvature is consistent with strong, nearly saturated Comptonization. Such strong Comptonization models have been invoked to explain the very high state of black hole binaries such as XTE 1550-564 (Done & Kubota 2006). However, the temperature derived for the electron plasma (~ 2 keV) is significantly lower than that of X-ray binaries (> 20 keV).

Another striking similarity between ULX and X-ray binaries is the presence of significant variability power as well as features in the power density spectra such as QPOs and breaks (Strohmayer & Mushotzky 2003; Dewangan et al. 2006; Mucciarelli et al. 2006; Strohmayer et al. 2007). The QPO and break frequencies are found to be smaller than those of X-ray binaries which is taken as evidence that ULX harbour IMBH. For some sources, like the ULX Holmberg II X-1, the variability is absent or very weak (Goad et al. 2006).

Studies of a collection of bright ULX in nearby galaxies reveal that for some ULX a power-law (PL) spectral fit (similar to the low/hard state of X-ray binaries) is adequate while others require a thermal component (similar to the high/soft state). The temperature of the thermal component is either ~ 0.2 or ~ 2 keV suggestive of a further subdivision (Winter et al. 2006; Devi et al. 2007). These studies do not indicate whether these spectral differences represent different spectral states or if ULX themselves are a heteroge-

neous class comprising different kinds of sources. Long term spectral variability, which is interpreted as state transitions similar to X-ray binaries, has been reported for several ULX (Kubota et al. 2001; La Parola et al. 2001; Fabbiano et al. 2003; Dewangan et al. 2004; Miyawaki et al. 2006; Feng & Kaaret 2006, 2007; Mizuno & et al. 2007; Fridriksson et al. 2008; Feng & Kaaret 2009a; Gladstone & Roberts 2009; Feng & Kaaret 2009b; Kajava & Poutanen 2009). Repeated *Chandra* observations of the Antennae have shown hardness ratio changes in several ULXs (Fabbiano et al. 2003). Transition from a high soft state to a low/hard state has been observed in two ULXs within IC 342 (Kubota et al. 2001) and Holmberg IX X-1 (La Parola et al. 2001). High/hard to low/soft spectral variability has also been observed from Holmberg II X-1 (Dewangan et al. 2004).

However, these spectral variations have not been shown to be associated with temporal behaviour changes and hence their identification as spectral state transitions similar to those observed in X-ray binaries remains uncertain. Moreover, the spectral variations recorded do not necessarily imply a change in the accretion disc geometry. Well constrained spectral parameters are needed for such an inference. Hence, study of long observations of bright ULXs undergoing state transition are crucial to ascertain whether ULX undergo true state transitions.

We investigate a possible state transition in a bright ULX in the spiral galaxy NGC 1313, located at a distance of 4.1 ± 0.1 Mpc (Méndez et al. 2002). The galaxy hosts three bright and well separated X-ray sources: two ULXs X-1 and X-2, and a supernova remnant SN 1978K. NGC 1313 X-1 is one of the first ULX observed by *XMM-Newton* to show soft X-ray excess emission that led to the $\sim 1000M_{\odot}$ IMBH interpretation (Miller et al. 2003). The ULX belongs to the low-temperature, high-luminosity class in the luminosity versus temperature ($L - kT$) diagram of bright ULXs in nearby galaxies (Feng & Kaaret 2005). Feng & Kaaret (2006, 2007) have utilised the first 14 *XMM-Newton* observations and reported long term spectral variations of the two ULXs NGC 1313 X-1 and X-2. For X-1, they fitted the spectra with an absorbed PL model and reported a correlation between the photon index, Γ and luminosity. An additional soft black body component was required for six of the observations. The short exposures of these observations (in the range of 9 – 41 ks), did not allow for detailed spectral and temporal studies.

Here we present detailed temporal and spectral properties of the ULX using two *XMM-Newton* observations of 123 and 20 ks. We describe the *XMM-Newton* observations and the spectral and temporal analysis in §2. In §3, the accretion disc geometries inferred from the analysis are described. We summarise and discuss the results in §4.

2 OBSERVATIONS AND DATA REDUCTION

We observed NGC 1313 with *XMM-Newton* for a 123 ks exposure on 15 October 2006 (observation identifier (obsid): 0405090101). NGC 1313 was also observed on 6 March 2006 with an exposure of 21.8 ks (obsid: 0301860101). Both observations were performed in the full frame mode of EPIC-pn and MOS cameras (Strüder & et al. 2001; Turner & et al. 2001) and using the medium filter. We used SAS 8.0.1 with

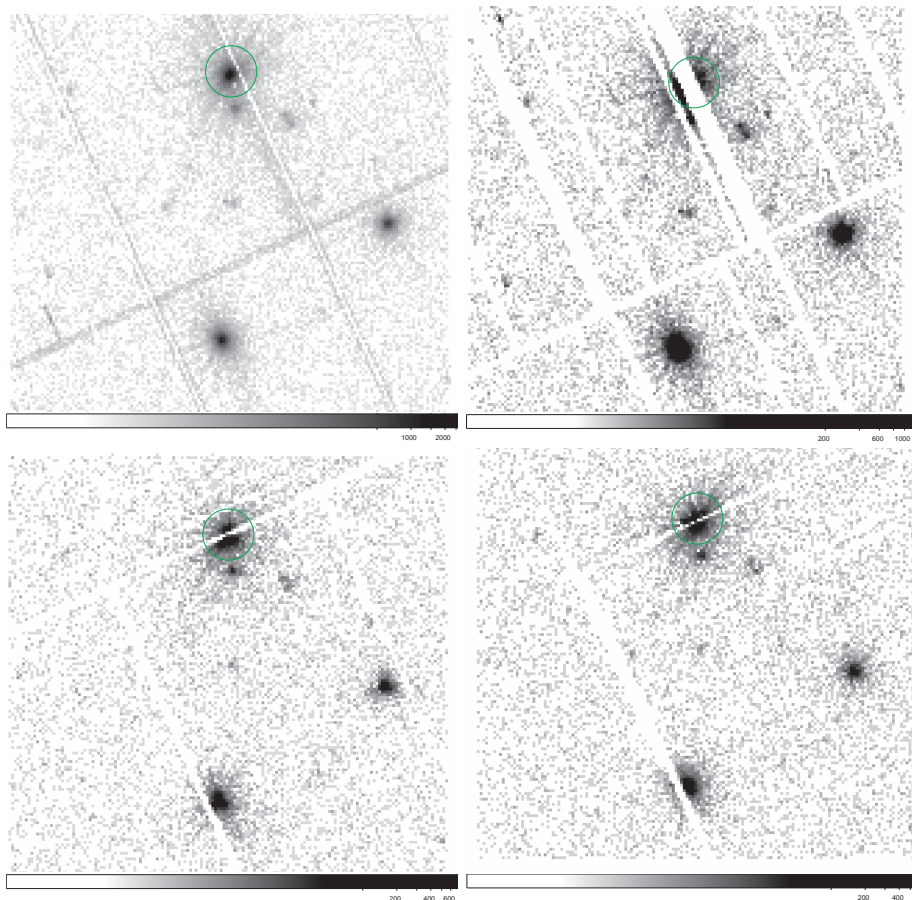


Figure 1. X-ray images of the region surrounding the ULX NGC 1313 X-1 extracted from the observation of 6 March 2006. The top left and right panels show EPIC-pn image extracted without and with FLAG=0 selection, respectively. The bottom left and right panels show MOS1 and MOS2 images extracted with FLAG=0 selection. The circular regions show the source extraction region. Clearly, a large fraction of EPIC-pn counts is lost with FLAG=0 selection for spectroscopy. Thus, EPIC-pn data without the FLAG=0 selection are best suited for timing analysis and the MOS1 & MOS2 data with the FLAG=0 selection are best suited for spectral analysis.

updated calibration to process and filter the EPIC-pn and MOS data. We used `epchain` and `emchain` to process the EPIC-pn and MOS data, respectively.

The long observation of 15 October 2006 was partly affected with low amplitude flaring particle background towards the end of the exposure. Cleaning of the flaring particle background and filtering for valid X-ray events (`#XMMEA_EP` or `#XMMEA_EM`, `PATTERN` ≤ 12 and `PI` in `[200:12000]`) resulted in a good exposures of 89.3, 89.4 and 89.5 ks for the EPIC-pn, MOS1 and MOS2 data, respectively. The ULX NGC 1313 X-1 resides well away from the CCD chip-gaps in both the pn and MOS camera data of the long observation.

On the other hand, the observation of 6 March 2006 was not affected by particle background, but the source resides on the chip-gaps in both the pn and MOS cameras. While the chip-gap in the pn data is 15.5 arcsec away from the source centroid, the chip-gap passes through the source centroid in the case of MOS data. Since the EPIC-pn camera has largest effective area and source is least affected with the chip-gap, we use pn data to study temporal variability. Specifically we selected events with patterns 0–12. For spectral analysis, the above selection criteria is not sufficient as all valid X-ray events are not accurately energy-calibrated.

In particular, events adjacent to the chip-gap have uncertain patterns due to the possible loss of charge in the chip-gap. Such events have less accurate energies and can be excluded with the selection criterion FLAG=0. For spectral analysis, thus we selected the events with pattern 0 – 4 (single and double) for the EPIC-pn and 0 – 12 for the MOS and excluded events adjacent to the chip-gaps and in columns with high offset with FLAG=0. Additionally, in the EPIC-pn observation of 6 March 2006, a few columns with high offset pass through the source. All the events in these columns have poor spectral calibration and hence were excluded from the spectral analysis. Thus a significant fraction of flux is lost in spectra generated from the March 2006 data. Note that the SAS task `arfgen` corrects for the loss of flux due to the excluded events adjacent to chip-gaps and in columns with high offset by reducing the effective area¹. In Figure 1, we show X-ray images with and without FLAG=0 selection for the observation. These images show loss of flux in the X-ray spectra as compared to that in lightcurves. Clearly, a large fraction of EPIC-pn counts is lost with the FLAG=0 selec-

¹ see SAS user guide available at http://xmm.esac.esa.int/external/xmm_user_support/documentation/sas_usg/USG/

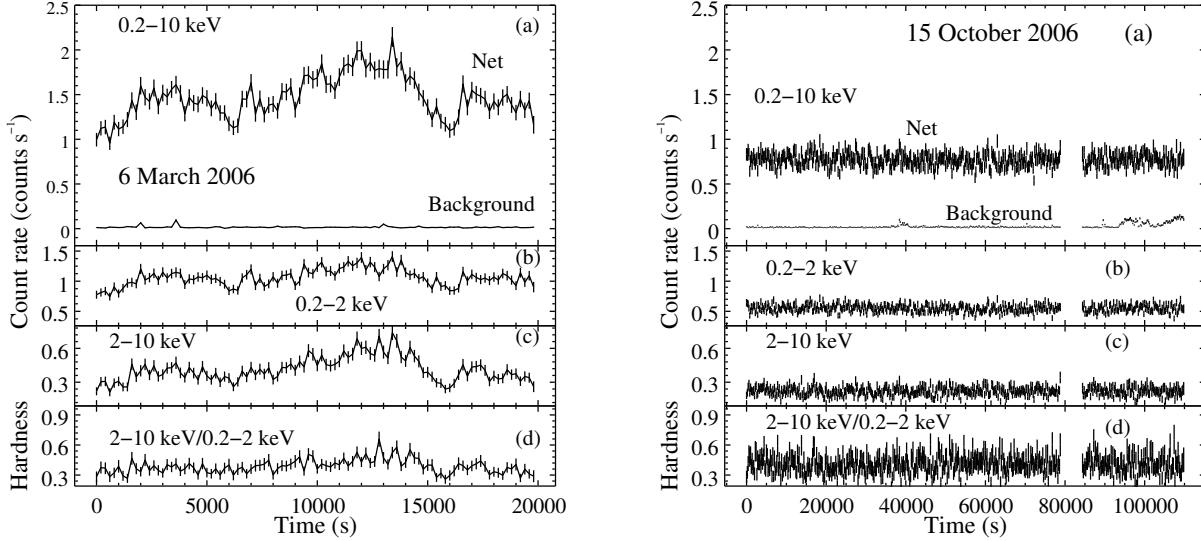


Figure 2. The background corrected EPIC-pn lightcurves of NGC 1313 X-1 binned with 200 s in the (a) 0.2 – 10 keV, (b) 0.2 – 2 keV, (c) 2 – 10 keV, and (d) the hardness ratio derived from the observations of 6 March 2006 (*left panel*) and 15 October 2006 (*right panel*). The relative contribution of background emission in the source extraction region is also shown for the 0.2 – 10 keV band.

tion. Thus the MOS1 & MOS2 data with the FLAG=0 selection and the EPIC-pn data without the FLAG=0 selection are best suited for spectral and timing analysis, respectively.

For both observations, we used a circular region of 40'' centred at the source position and extracted the spectra and lightcurves for the ULX. We also extracted the background lightcurves and spectra using circular regions in source-free areas but close to the source. We created spectral response files using the SAS tasks `rmfgen` and `arfgen`.

2.1 Temporal Analysis

We used EPIC-pn data without the FLAG=0 selection for the timing analysis. We extracted two sets of lightcurves from each of the observations with bin sizes of 200 s and 0.5 s. In Figure 2, we show the background corrected lightcurves of NGC 1313 X-1 in the 0.2 – 10 keV, 0.2 – 2 keV and 2 – 10 keV bands. For comparison, we have also plotted the background contribution in the source extraction region. Evidently background contribution is nearly constant and negligible throughout the observations.

As can be seen in Fig. 2 (*left panel*), NGC 1313 X-1 showed strong X-ray variability throughout the observation of 6 March 2006. The most remarkable variability in the 0.2 – 10 keV band occurred at an elapsed time of ~ 13000 s when the net count rate decreased by a factor of about two in 3000 s. The hardness ratio (HR), calculated as the ratio of count rates in the 0.2 – 2 keV and 2 – 10 keV band is also variable and correlated with the lightcurve. A constant model fit to the hardness-ratio curve resulted in $HR = 0.37$ with a minimum $\chi^2 = 157.3$ for 99 degrees of freedom. The spectrum of the ULX hardens with increasing flux.

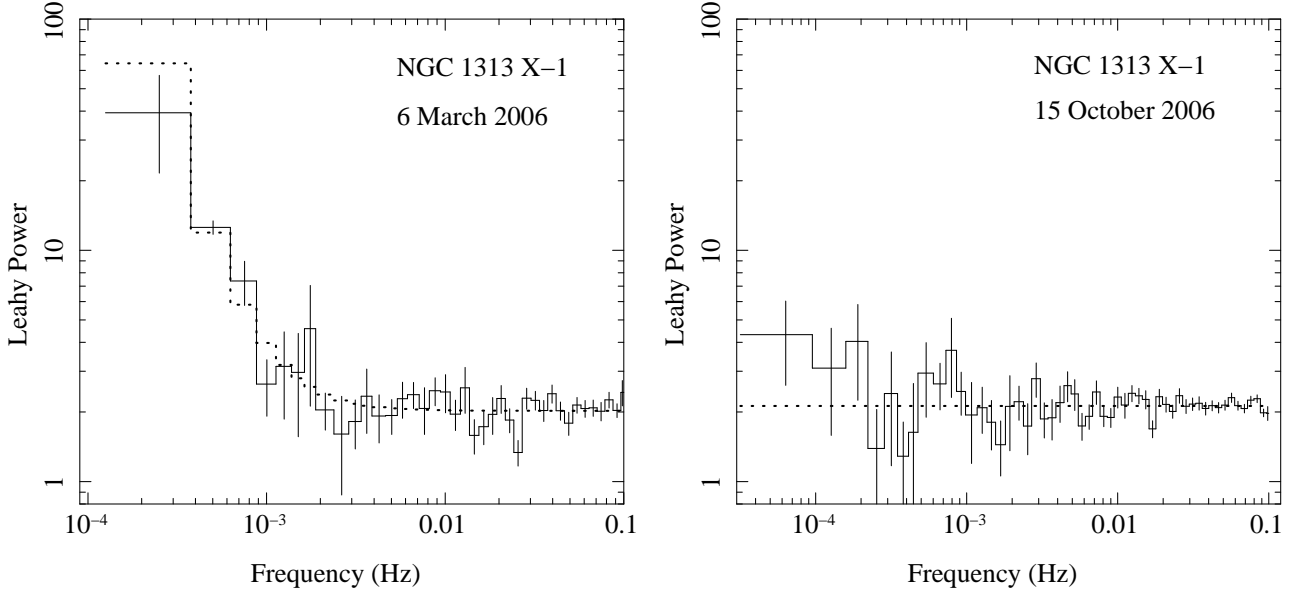
In contrast to the 20 ks observation on 6 March 2006, the long observation of 15 October revealed that (*i*) the ULX

was in a low flux state, X-ray emission dropped by a factor of about ~ 2 , and (*ii*) the emission was remarkably steady throughout the ~ 120 ks exposure. The soft and hard band emission and the hardness ratio also remained steady, implying that the spectrum of the ULX did not change substantially (see Fig. 2, *right panel*). Henceforth, throughout this work we refer to the 6 March observation as the high flux state and the 15 October one as the low flux state.

To quantify the variability, we have calculated the intrinsic source variability expressed in terms of the fractional variability amplitude $F_{var} = (\sigma_{XS}^2 / \bar{x}^2)^{1/2}$, where σ_{XS}^2 is the variance after subtracting the contribution expected from measurement errors, and \bar{x} is the mean count rate (see Vaughan et al. 2003, and references therein). We used the background corrected lightcurves binned with 200 s to calculate F_{var} , listed in Table 1. While the measured F_{var} is consistent with no intrinsic variability during the low flux state, significant intrinsic variability is seen during the high flux state. We have also derived the power spectral density (PSD) from the EPIC-pn lightcurves binned with 0.5 s. We used the `powspec` program to rebin the lightcurves to 5 s bins and calculated the PSD. For the low flux state, we used the first ~ 79 ks continuous exposure in order to avoid the data gap and the flaring particle background seen towards the end of the observation (see Fig. 2). The light curves were divided into five equal segments and the PSDs of each segment was computed. The five individual PSDs were averaged and the errors were assigned to be the standard deviation at each frequency bin. The resultant PSDs were binned by a factor of 1.1 in frequency and are shown in Figure 3. We used the Leahy normalisation so that power due to Poisson noise is 2 which was not subtracted from the resulting PSDs. The PSD shows red-noise behaviour at low frequencies and constant power arising from the Pois-

Table 1. Variability properties of NGC 1313 X-1

Energy band	6 March 2006			15 October 2006		
	Source (counts s ⁻¹)	Background (counts s ⁻¹)	$F_{var}(\%)^1$	Source (counts s ⁻¹)	Background (counts s ⁻¹)	$F_{var}(\%)^1$
0.2 – 10 keV	1.47 ± 0.09	0.016 ± 0.004	14.6 ± 0.6	0.77 ± 0.07	0.026 ± 0.006	2.3 ^{+0.9} _{-1.9}
0.2 – 2 keV	1.06 ± 0.08	0.009 ± 0.003	11.0 ± 0.8	0.55 ± 0.06	0.010 ± 0.004	2.9 ^{+1.0} _{-1.7}
2 – 10 keV	0.41 ± 0.05	0.006 ± 0.003	23.7 ± 1.2	0.22 ± 0.04	0.013 ± 0.004	< 4.3

¹Calculated from background subtracted lightcurve with 200 s bins.

Figure 3. Power density spectra of NGC 1313 X-1 derived from the EPIC-pn lightcurves obtained on 6 March 2006 and 15 October 2006

son noise at high frequencies in the high flux state, while it is flat, dominated by Poisson noise, during the low flux state. A constant model fitted to the PSD for the low flux state resulted in a minimum $\chi^2 = 59.3$ for 52 degrees of freedom (dof). The best-fit constant power density is 2.12 ± 0.04 which is slightly higher than the power density of 2 expected from pure Poisson noise arising from photon counting statistics. The marginal higher power density could arise from slight variation in the background level (see Fig. 2 *right panel*). Thus, we measure no significant intrinsic variability, consistent with the measured F_{var} (see Table 1). As expected, a constant power density model fit to the PSD of the high flux state resulted in a statistically unacceptable fit ($\chi^2/dof = 211.5/38$). A PL component ($\propto \nu^{-\alpha}$) plus a constant model to account for the Poisson noise improved the fit significantly ($\chi^2/dof = 47.7/36$) with $\alpha = -2.25 \pm 0.30$. Interestingly a broken PL and constant model further improved the fit marginally ($\chi^2/dof = 40.9/34$). However, the parameters of the model are not well constrained and hence we conclude that the data is suggestive of a break, but no concrete inference can be made. Long observations of the ULX in the high flux state are required to measure the break frequency.

2.2 Spectral Analysis

We used EPIC-pn and MOS data with the FLAG=0 selection for the spectral analysis. Spectral bins were chosen such that there was a minimum of 20 counts per spectral channel for the pn and the MOS data of March 2006 (high flux state). The high signal-to-noise EPIC-pn, MOS1 and MOS2 data extracted from the deep observation of October 2006 (low flux state) were grouped to minimum counts of 200, 50 and 50, respectively. These spectra were analysed with *ISIS 1.4.9*. All spectra were fitted in the energy range 0.3 – 10 keV and the errors on the best-fit spectral parameters are quoted at a 90% confidence level.

We begin with the spectral analysis of the low flux state. A simple absorbed PL (*wabs*powerlaw*) model was fitted individually to the pn and MOS spectra. Examination of the individual fits showed that the photon indices and absorption columns obtained for three data sets were similar within errors and the fits had similar residuals. Therefore, we fitted the pn and MOS data jointly and used an overall normalisation constant to account for possible differences in source extraction areas or calibration uncertainties. The absorbed PL model resulted in an statistically unacceptable fit ($\chi^2/dof = 1484.0/674$). The ratio of the pn+MOS data and the PL model is shown in Fig. 4 (*bottom panel*). This plot clearly shows a broad hump or a cutoff near 6 keV and

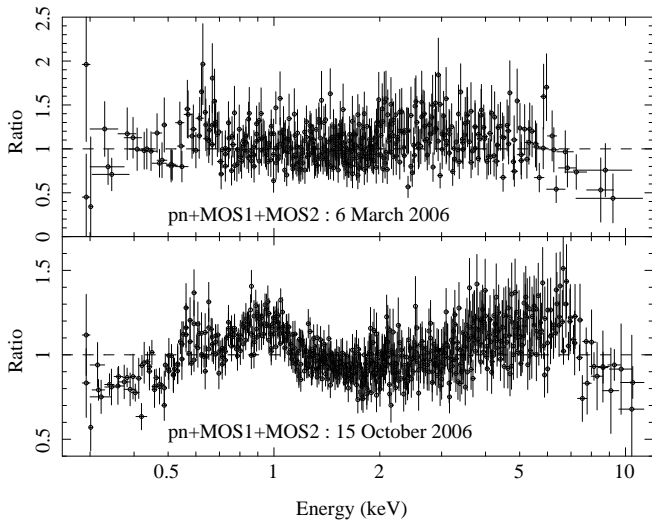


Figure 4. Ratios of observed pn+MOS data obtained on 6 March 2006 (*top panel*) and 15 October 2006 (*bottom panel*) and the best-fitting absorbed PL models.

a soft X-ray hump or excess emission in the 0.6 – 1.2 keV band. Similar spectra have been reported earlier for several ULXs (Feng & Kaaret 2005; Stobbart et al. 2006; Dewangan et al. 2006). Addition of a multicolour disc blackbody (MCD; the `diskbb` model in XSPEC) component to the PL model improved the fit significantly ($\chi^2/dof = 807/672$) with $kT_{in} = 0.20 \pm 0.01$ keV and $\Gamma = 1.71 \pm 0.02$. Replacing the PL with a cutoff PL (`cutoffpl`) further improved the fit ($\chi^2/dof = 717.3/671$) with a cutoff energy, $E_{cutoff} = 5.9^{+1.4}_{-1.0}$ keV and $\Gamma = 1.0^{+0.15}_{-0.16}$. This kind of a high energy cut-off is common among bright ULXs and is well described by thermal Comptonization in a relatively cool and optically thick plasma. (Agrawal & Misra 2006; Stobbart et al. 2006; Goad et al. 2006; Dewangan et al. 2006; Roberts 2007). To test such a scenario, we replaced the cutoff PL model with the thermal Comptonization model (`nthcomp`) described by Zdziarski et al. (1996) and Życki et al. (1999). The free parameters of the `nthcomp` model are the asymptotic PL index (Γ_{thcomp}), electron temperature (kT_e) and the seed photon temperature (kT_s). The electron scattering optical depth (τ) can be calculated from the asymptotic PL photon index (Γ_{thcomp}) and electron temperature (kT_e) as follows (Sunyaev & Titarchuk 1980)

$$\Gamma_{thcomp} = \left[\frac{9}{4} + \frac{1}{(kT_e/m_e c^2)\tau(1 + \tau/3)} \right]^{1/2} - \frac{1}{2} \quad (1)$$

Note that the optical depth τ is a geometry dependent quantity and will differ for a spherical or a slab one.

Since a soft X-ray excess emission, described by an MCD, is clearly detected, it is simplistic to assume that this component provides the seed photons for the Comptonization. Therefore, the temperature of the soft excess and the seed photons were kept the same and varied together. The shape of the soft component was assumed to be that of a MCD. The `MCD+nthcomp` model provided a good fit ($\chi^2/dof = 717.9/671$) and the best-fit parameters are reported in Table 2. In Fig. 5, we show the unfolded EPIC-pn spectrum, the best-fitting absorbed `MCD+ncomp` model in panel (a) (*lower curve*, marked with 15 Oct 2006), and

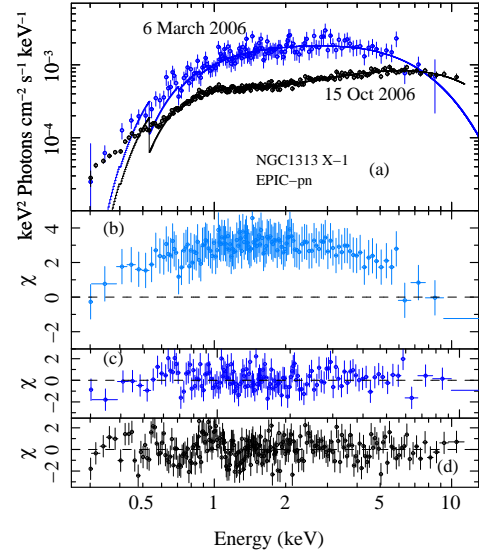


Figure 5. Results of spectral fitting to the EPIC-pn data in the high and low flux states. (a) *Upper plot*: Unfolded spectrum in the high flux state (6 March 2006) and the best-fit model - thermal Comptonization in a cool, optically thick medium; *lower plot*: Unfolded spectrum in the low flux state (15 October 2006) and the best-fit model `MCD+nthcomp`. *The apparent departure of the unfolded data from the best-fit models at low energies are not real but due to the fact that the unfolded spectra have been derived in a model independent way (see text for detail)*. (b) Deviations of the observed data in the high flux data from the best-fit model. (c) Deviations of the observed data of the high flux state from the best-fit absorbed `nthcomp` model. (d) Deviations of the observed data for the low flux state from the best-fit absorbed `MCD+nthcomp` model.

the deviations of the data from the model in panel (d). For clarity we show only the EPIC-pn data. Unlike XSPEC, the unfolded spectrum in ISIS is derived in a model-independent way as follows:

$$f_{unfold}(I) = \frac{[C(I) - B(I)]/\Delta t}{\int R(I, E)A(E)dE}, \quad (2)$$

where $C(I)$ is the number of total counts in the energy bin I , $B(I)$ is the number of background counts, Δt is exposure time, $R(I, E)$ is the normalised response matrix and $A(E)$ is the effective area at energy E . This definition produces a spectrum that is independent of the fitted model. The best-fit model has been over-plotted at the internal resolution of the ancillary response function. The data and the model are expected to match only in the particular case of unit response matrix (Nowak 2005). Hence there is deviation between the model and the data points at low energies. Note that the *model independent* unfolded data points clearly shows a curvature at high energies, which signifies that the curvature is real and not a modelling artifact.

We then proceed to the spectral analysis of the pn and MOS data of the high flux state. Simple absorbed PL model fitted separately to the pn, MOS1 and MOS2 data resulted in similar photon indices and we did not find significant differences in the residuals, therefore we present results based on joint spectral fitting of the pn and MOS data as before.

Table 2. Best-fit spectral model parameters for NGC 1313 X-1.

Parameters	6 March 2006 nThComp	15 October 2006 MCD+nThComp
$N_H(10^{21} \text{ cm}^{-2})$	2.50(fixed)	$2.50_{-0.15}^{+0.16}$
$kT_{in}(\text{ eV})^a$	–	227
f_{MCD}^b	–	$1.24_{-0.12}^{+0.15} \times 10^{-12}$
$kT_S(\text{ eV})^c$	122 ± 15	227_{-12}^{+14}
$kT_e(\text{ keV})^d$	1.7 ± 0.2	$2.27_{-0.15}^{+0.18}$
Γ_{thcomp}^e	$2.02_{-0.04}^{+0.05}$	1.67 ± 0.03
τ^f	$13.5_{-1.5}^{+1.4}$	$15.1_{-1.0}^{+1.1}$
f_{comp}^g	$(7.5 \pm 0.2) \times 10^{-12}$	$(3.1 \pm 0.1) \times 10^{-12}$
f_X^h	$(7.5 \pm 0.2) \times 10^{-12}$	$(4.3 \pm 0.2) \times 10^{-12}$
L_{bol}^i	1.7×10^{40}	1.2×10^{40}
χ_{min}^2/dof	421.4/439	717.9/671

^aInner disc temperature of disc blackbody model which is tied to kT_S .

^b0.3 – 10 keV flux of the MCD component in $\text{ergs cm}^{-2} \text{ s}^{-1}$.

^cTemperature of the seed photon source of the Comptonization model

^dHot electron plasma temperature.

^ePhoton Index of the Comptonization model.

^fOptical depth τ derived from kT_e and Γ_{thcomp} using the Equation 1.

^g0.3–10 keV flux of the Comptonization model in $\text{ergs cm}^{-2} \text{ s}^{-1}$.

^hUnabsorbed 0.3 – 10 keV flux in $\text{ergs cm}^{-2} \text{ s}^{-1}$ calculated from the MOS1 data.

ⁱUnabsorbed bolometric luminosity in ergs s^{-1} .

The absorbed PL model resulted in a minimum $\chi^2 = 455.3$ for 440 dof. With a reduced $\chi^2 = 1.03$, an absorbed PL model seems adequate and does not seem to warrant exploration of more complex models. Indeed Feng & Kaaret (2006) were able to model several similar quality data of this source with an absorbed PL. However, the analysis of better quality data described above suggests that the spectrum of the source could be more complex. Moreover, as we show below, there is evidence for a more complex spectral shape even for this statistically poorer data set. We have plotted the ratio of the pn+MOS1+MOS2 data and the best-fit PL model in Figure 4(*upper panel*). The absorbed PL model is a good description of the data below ~ 6 keV. There is a likely cutoff or curvature at high energies. To verify the possible high energy turnover of the X-ray spectra, we replaced the PL component by a cut-off PL. The absorbed cut-off PL model yielded $\Delta\chi^2 = -19.9$ for one additional parameter as compared to the absorbed PL model. This is an improvement at a significance level of $> 99.99\%$ based on the Maximum Likelihood Ratio test. The absorbed nthcomp model provided a similar fit with $\chi^2/\text{dof} = 421.4/439$. In Fig. 5, we show the unfolded EPIC-pn spectrum, the best-fitting absorbed nthcomp model in panel (a) marked as 6 March 2006 and the deviations in panel (c). Note that, similar to

the low flux state data set, the *model independent* unfolded data points clearly show a curvature at high energies which again signifies that the curvature is real and not a modelling artifact. It is also clear from the model independent unfolded data that both the flux and spectral shape varied between the two data sets. We show spectral variability in panel (b) of Fig. 5 which shows the deviations of the high flux state data from the best fit model of the low flux state. We list the parameters of the best-fit absorbed nthcomp model in Table 2. We have also investigated the possible presence of a disc component similar to that observed in the low flux state. Addition of an MCD component to the nthcomp model with MCD kT_{in} tied to the nthcomp kT_S did not improve the fit. We calculated an upper limit of $L_{MCD} < 1.4 \times 10^{39} \text{ ergs s}^{-1}$ for the bolometric luminosity of the MCD component in the 0.001 – 100 keV band. We also fixed the MCD kT_{in} at the value obtained for the low flux state and calculated the upper limit, $L_{MCD} < 6.3 \times 10^{39} \text{ ergs s}^{-1}$.

3 ACCRETION DISC GEOMETRY

As revealed in Table 2, the low flux state spectrum of the source can be described with a thermal Comptonization and a disc black body model. The luminosity of the disc black body (i.e. the MCD model) is $L_{MCD} \sim 4 \times 10^{39} \text{ ergs s}^{-1}$, while that of the thermal Comptonization is $\sim 7.7 \times 10^{39} \text{ erg s}^{-1}$. Using the XSPEC model function (`nthcomp.f`) for the model nthcomp, one can estimate the amplification factor, $A \equiv L_c/L_s \sim 4.8$, where L_c and L_s are the luminosities of the Comptonization component and the seed photon input. This allows an estimate of $L_s \sim 1.6 \times 10^{39} \text{ erg s}^{-1}$. This is consistent with an accretion disc geometry where a standard cold accretion disc is terminated at radius R_{tr} and the inner region is a hot plasma. The inner hot plasma Comptonizes photons from the outer disc producing high energy photons. For consistency, the seed photon spectral shape for the Comptonization model is taken to be a disc black body emission at the same temperature as the disc emission observed. In this model, the fraction of the cold disc photons that enter the inner hot region is related to the solid angle which the hot region subtends from the outer disc. The observed fraction of the luminosity of the seed photon component as compared to the disc luminosity, $L_s/L_{MCD} \sim 0.4$ suggests a solid angle of $\Delta\Omega \sim 0.4 \times 2\pi \sim 0.8\pi$. Note that $L_s/L_{MCD} \lesssim 1$ is a consistency check for the geometry proposed. In this geometry, it would be difficult to reconcile $L_s > L_{MCD}$ and $L_s \ll L_{MCD}$ would require an unphysical small subtending solid angle.

The normalisation of the disc component provides an estimate of the transition radius

$$R_{tr} \sim 10^9 \text{ cm} \left(\frac{\kappa}{1.7} \right)^2 \left(\frac{\cos i}{0.5} \right)^{-1/2} \quad (3)$$

where i is the inclination angle and κ is the colour factor. In the standard accretion disc theory (Shakura & Sunyaev 1973), the luminosity of a truncated disc is given by

¹ In this section all luminosities are the unabsorbed values.

$$L_{MCD} \sim \frac{3GM\dot{M}}{2R_{tr}} \quad (4)$$

where M is the mass of the black hole and \dot{M} is the accretion rate. The total bolometric luminosity, $L_T = (L_C - L_S) + L_{MCD}$ can be expressed as $L_T = \eta\dot{M}c^2$ where η is the efficiency of the system. Thus, the mass of the black hole can be estimated to be

$$\begin{aligned} M &\sim \frac{2c^2}{3G} \eta R_{tr} \frac{L_{MCD}}{L_T} \\ &\sim 200 M_\odot \left(\frac{\eta}{0.1}\right) \left(\frac{R_{tr}}{10^9 \text{cm}}\right) \left(\frac{L_{MCD}/L_T}{0.4}\right) \end{aligned} \quad (5)$$

The Eddington luminosity for a $200M_\odot$ black hole is $L_{Edd} = 2.5 \times 10^{40} \text{ erg s}^{-1}$ and hence the source is radiating at an Eddington ratio of $L_T/L_{Edd} \sim 0.37$. The Schwarzschild radius turns out to be $r_s \equiv 2GM/c^2 \sim 6 \times 10^7 \text{ cm}$, making the transition radius $R_{tr} \sim 17r_s$.

Thus the spectral shape of the low flux state is totally consistent with a scenario where a $\sim 200M_\odot$ black hole is surrounded by a standard accretion disc which is truncated at $\sim 17r_s$. The disc produces a multi temperature emission which is observed as a soft component. The inner hot region is geometrically thick and subtends a solid angle of $\sim 0.8\pi$ to the disc outside. This allows it to Comptonize photons from the outer disc producing the main Comptonized component. The system is radiating at a Eddington ratio ~ 0.4 for a standard radiation efficiency $\eta \sim 0.1$.

The spectrum of the high flux state can be adequately fitted with a single thermal Comptonization model. The luminosity of the model is $\sim 1.7 \times 10^{40} \text{ erg s}^{-1}$ and the amplification factor, $A \sim 2.5$. The input seed photon luminosity turns out to be $\sim 6.5 \times 10^{39} \text{ erg s}^{-1}$. This is significantly higher by a factor of ~ 4 of the seed photon luminosity for the low flux state. If, like in the low flux state, the seed photons are due to an external truncated accretion disc, the direct emission from such a disc is expected to be $L_{MCD} \sim \frac{L_S}{0.4} \sim 1.6 \times 10^{40} \text{ ergs s}^{-1}$ which would have been easily detected. The upper-limit to the observed disc emission, however, is only $6.3 \times 10^{39} \text{ ergs s}^{-1}$. Thus the absence of a soft component in the spectrum argues against such a geometry. Moreover, if the input seed photon shape is taken as disc black body emission, the inner disc temperature turns out to be 0.2 keV which is similar to that of the low flux state, despite the factor of four change in luminosity. The luminosity of a truncated accretion disc is $\propto \dot{M}/R_{tr}$ while the temperature is $\propto \dot{M}^{1/4}/R_{tr}^{3/4}$. Thus a near constant temperature accompanied by a factor of four increase in luminosity would imply that the accretion rate \dot{M} has increased by a factor of ~ 8 while the truncation radius has increased by a factor of ~ 2 . The large factor of ~ 8 change in the accretion rate is not reflected in the change in the total luminosity of the source, which is only a factor of ~ 1.5 higher than the low flux state. Thus a truncated accretion disc with an inner hot region does not seem to be a viable model for the high flux state of the source.

An alternate geometry for the high flux state spectrum is that of a corona covering an optically thick and geometrically thin disc (Liang & Price 1977; Svensson & Zdziarski 1994; Haardt & Maraschi 1993). In this sandwich model, a fraction of the total gravitational power is dissipated in the disc, P_d and the rest in the corona P_c . The disc photons

get Comptonized by the overlying corona and hence only a thermal Comptonized spectrum is observed. A fraction ξ of the Comptonized photons impinge back on to the underlying disc and are absorbed. The luminosity of the seed photon is then $L_s = P_d + \xi L_c$, where L_c is the luminosity of the Comptonized photon. The observed total luminosity $L_o = L_c(1 - \xi) = P_d + P_c$. Defining the Compton amplification factor $A \equiv L_c/L_s$, the dissipated powers can be related to the total luminosity as,

$$P_c = \frac{A - 1}{(1 - \xi)A} L_o \quad (6)$$

and

$$P_d = \frac{1 - \xi A}{(1 - \xi)A} L_o \quad (7)$$

The geometry is valid only for $\xi < \xi_{max} = 1/A$. In the absence of feedback, $\xi = 0$, $P_d = L_o/A$ and $P_c = L_o - P_d$. In the other extreme of maximal feedback $\xi = \xi_{max}$, $P_d = 0$ and $P_c = L_o$.

For the high flux state, the spectrum can be interpreted in terms of the corona model, with the seed photon luminosity assumed to be a black body. The seed photon temperature turns out to $\sim 0.12 \text{ keV}$ and an amplification factor of $A \sim 2.5$ which imposes an upper limit on $\xi_{max} \sim 0.4$. Thus with a $\xi \lesssim 0.4$ and absence of any other strong soft component, the spectrum is consistent with the corona model. The size of the corona region R_c can be estimated using $\sigma T_s^4 2\pi R_c^2 = L_s = L_o/(1 - \xi)A$, where T_s is the temperature of the underlying disc. For $L_o \sim 1.7e40 \text{ erg s}^{-1}$, $\xi \sim 0.25$ and $A \sim 2.5$, $R_c \sim 3 \times 10^9 \text{ cm}$. For a $200M_\odot$ black hole this corresponds to $\sim 50r_s$. If there is an standard accretion disc beyond this radius, its temperature would be $< 0.1 \text{ keV}$ and would have a luminosity $< 2 \times 10^{39} \text{ erg s}^{-1}$. Such a emission would not have been detected. The Eddington ratio for this flux state turns out be ~ 0.7 as compared to ~ 0.4 for the low one.

The temporal variability of the high flux state spectrum allows us to further constrain and verify the corona geometry. The fractional root mean squared (rms) variability as a function of energy is shown in Figure (6). The simplest interpretation would be that the observed variability is induced by variations in the coronal power P_c . From equations (6) and (7), the amplification can be written as

$$A(T_e, T_s, \tau) = \frac{P_d + P_c}{P_d + \xi P_c} \quad (8)$$

where T_e is the corona temperature and the seed photon luminosity as

$$L_s = \frac{P_d + \xi P_c}{1 - \xi} \propto T_s^4 \quad (9)$$

A variability in $P_c(t) = P_{c0}(1 + \delta P_c(t))$, will induce corresponding variation in the amplification, δA and the seed photon temperature δT_s . Assuming that the optical depth τ of the corona does not vary, the above two equations determine the time variability of $T_e(t)$ and $T_s(t)$ as a function of $\delta P_c(t)$. The time dependent spectrum can then be obtained from $T_e(t)$ and $T_s(t)$. The standard deviation of the time dependent spectrum at different energy bands then provides a predicted rms variation that can be compared with the observed values (Gierliński & Zdziarski 2005). For $\xi = 0.25$ (solid line in Figure 6), the predicted curve is consistent with

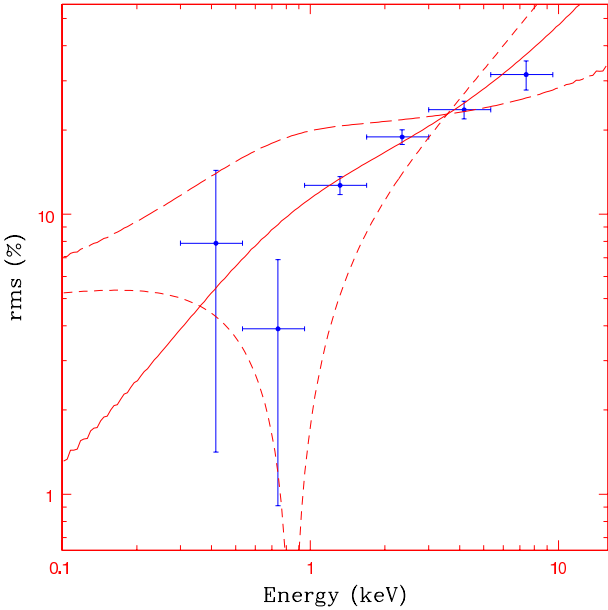


Figure 6. The observed rms variation with energy for the high flux state data. The predicted rms variation for $\xi = 0.25$ (solid line), $\xi = 0$ (dashed line) and for $\xi = \xi_{max} = 0.4$ (long dashed line).

the observations. For comparison, curves for $\xi = 0$ (dashed line) and $\xi = \xi_{max} = 0.4$ (long dashed line) are also plotted in the figure. Note that apart from the overall normalisation, the predicted rms versus energy plot depends only on ξ , since the rest of the parameters are determined by the time-averaged spectral fitting. Thus the coronal geometry naturally explains the energy dependent variability of the source.

As the coronal power increases, the electron temperature should also increase making the spectrum harder. Thus the model predicts a correlation between flux and hardness ratio which is indeed seen in the variability. In the left panel of Figure (2) the hardness ratio is observed to increase with flux. While the qualitative behaviour is consistent, a quantitative evaluation is unfortunately not possible. Such a quantitative estimate would require a fairly accurate knowledge of the response of the instrument to convert the model photons into counts. As mentioned earlier, for this observation, the source extension overlaps with the EPIC-pn chip gap and a large fraction of events have uncertain pattern. These events with poor spectral calibration, although excluded from the spectral analysis, were included in the temporal analysis. Excluding them from the temporal analysis renders the statistics too poor but their inclusion means that their energies are not well constrained.

The spectrum and rms variability of the source in the high flux state is totally consistent with a geometry where a corona covers an underlying disc in a sandwich model. The photons emitted from the disc are Comptonized by the corona and only a single thermal component is seen. The size of the coronal region is $\sim 50r_s$ for a $200 M_\odot$ black hole and the Eddington ratio is ~ 0.7 .

The model requires a fraction $\xi \sim 0.25$ of the Comptonized photons impinge back on the disc and are ab-

sorbed. In principle, this fraction should be computed self-consistently for the specific geometry and spectral parameters by using a Monte Carlo code. The simple sandwich geometry where the corona is a geometrically thin layer on top of a cold accretion disc will probably not be viable, since for an optically thick layer, ξ should be $\lesssim 1$. A possible model could be that the Comptonizing region is an inner spherical cloud and the soft photon source is a thin accretion disc which extends only partially into the cloud. Alternatively, the soft photon source may be a small annular inner disc, surrounded by the spherical Comptonizing region. Detailed modelling taking into account the radiative constrains as well as dynamics of the inner region needs to be undertaken to verify the correct geometry for such sources.

4 SUMMARY AND DISCUSSION

We have investigated the spectral and temporal behaviour of the bright ULX NGC 1313 X-1 using two *XMM-Newton* observations. On 6 March 2006, the ULX was in a high flux state with an average EPIC-pn count rate of ~ 1.5 counts/s, while on in October 2006 the count rate had decreased to ~ 0.78 counts/s. The main results of the analysis are as follows.

The spectrum of the low flux state shows definite evidence for a high energy curvature. It can be fitted with a thermal Comptonization model with an optical depth $\tau \sim 15$ and temperature $kT_e \sim 2.3$ keV. An additional soft component, which can be modelled as a disc black body emission with a inner disc temperature of $kT_{in} \sim 0.23$ keV, is required for the spectral fit. The flux from the source is steady (i.e. no variability is detected at a significance greater than 2σ) with an upper limit on the rms variability of $< 3\%$.

The spectral shape during the high flux state is distinctively different from that of the low flux state. The entire spectrum can be fitted by a single thermal Comptonization model with an optical depth $\tau \sim 13.5$ and temperature $kT_e \sim 1.7$ keV. There is no evidence for any additional soft component. The source is highly variable in this flux state with an rms variability of 14%. The associated temporal and spectral difference between the two observations indicates that the source underwent a true state transition.

For a standard radiative efficiency of ~ 0.1 , the spectrum of the low flux state is completely consistent with a model where a $\sim 200M_\odot$ black hole is surrounded by a standard accretion disc truncated at a radius of $\sim 17r_s$ ($r_s \equiv 2GM/c^2$). This outer disc gives rise to the soft component. There is an inner hot region which subtends a solid angle of $\sim 0.8\pi$ to the outer disc. Hence photons from the outer disc enter the inner hot region, get Comptonized, and are observed as the primary thermal Comptonized component. The system has an Eddington ratio of $L_T/L_{Edd} \sim 0.4$.

The spectrum of the high flux state is not compatible with a truncated disc and inner hot region geometry. This is primarily inferred by the absence of any strong soft component, despite a four fold increase in the input soft photon flux at nearly the same temperature. The difference in disc geometry further confirms that a true state transition has occurred between the two observations.

The spectrum as well as *the rms variability as a function of energy* of the high flux state, is completely consistent with

a model where a Comptonizing region completely covers the geometrically thin disc. Photons from the disc get Comptonized in the corona and a single thermal Comptonization model is observed. The model requires a fraction ~ 0.25 of the Comptonized photons to impinge back on the disc and be absorbed. The observed variability can be naturally ascribed to variations in the coronal power. The size of the coronal region is $\sim 50r_s$ and the Eddington ratio during this flux state is ~ 0.7 .

The low flux state of NGC 1313 X-1 seems to be analogous to the low/hard state of Galactic X-ray binaries, which can also be broadly explained in terms of a truncated accretion disc and an hot inner region. Similarly the coronal geometry for the high flux state is related to the one invoked for the high soft state of Galactic X-ray binaries. However, this is an important difference between the hot region/corona of Galactic sources and NGC 1313 X-1. The hot region/corona of Galactic sources is optically thin ($\tau \sim 1$) and has a high temperature, ~ 50 keV. The hot region/corona for NGC 1313 X-1, is optically thick ($\tau \gtrsim 10$) and has a much lower temperature ~ 2 keV. This difference is more than just quantitative. Optically thin plasmas with electron temperatures ~ 50 keV can be in a two-temperature state, with the proton temperature being much higher (a factor of ~ 1000) than that of the electron gas (Shapiro et al. 1976). Such plasmas are gas pressure dominated. Optically thick and low temperature plasmas cannot have such a two-temperature structure and would be radiation pressure dominated. Thus, such plasmas would have to be dynamically different from those observed in Galactic sources.

In contemporary works, Heil et al. (2009) and Gladstone et al. (2009) have analysed the long October data of NGC 1313 X-1. Heil et al. (2009) have reported white noise like variability with a break at ~ 0.1 Hz. This is consistent with the power spectrum reported here Figure 3. As noted by Heil et al. (2009), the identification of a break at > 0.1 Hz requires a careful estimate of the noise level. Gladstone et al. (2009) have analysed the spectrum and found that the best fit interpretation is that of a disc black body and a Comptonized spectrum. The best fit parameters are similar to the ones obtained here with $kT_S \sim 0.27$ keV, optical depth $\tau \sim 17$ and a ratio of the Comptonized to seed photon luminosity to be ~ 4 . Taking into account spectral analysis of several other ULX, they suggest that the generic geometry is that of a standard accretion disc covered by a hot corona. Here, the same geometry is used to explain the spectral properties and temporal behaviour for the 6th March, high flux data. On the other hand, for the low flux October data we favour a geometry where the standard disc is truncated and there is an hot inner region.

With an Eddington ratio of ~ 0.5 , the only difference between NGC 1313 X-1 and Galactic black hole systems seems to be the larger mass of the black hole. However, the X-ray spectra of bright AGN reveal the presence of an optically thin and hot plasma similar to those inferred for Galactic sources. It is not clear why AGN with a $\sim 10^{6-9} M_\odot$ black hole mass have similar hot region/corona as $\sim 10 M_\odot$ Galactic black holes, but ULX with intermediate masses have qualitatively different plasmas. The broadband X-ray spectra of BHBs in their strongly Comptonized, very high state (VHS) require thermal Comptonization in an optically

thick ($\tau \sim 2-3$) and relatively cool ($kT_e \sim 10$ keV) plasma in addition to multi-colour disc blackbody emission from a truncated disc and a PL extending to high energies (Done & Kubota 2006). The curvature produced by the low temperature thermal Comptonization component in BHBs could be similar to the ~ 5 keV curvature seen in the ULX spectra. Furthermore, many narrow-line Seyfert 1 galaxies and quasars with high Eddington ratio show soft X-ray excess emission with $kT \sim 200$ eV above a hard PL. The soft excess emission can be modelled with thermal Comptonization in an optically thick and cool plasma (see e.g., Magdziarz et al. 1998; Dewangan et al. 2007; Middleton et al. 2009). Perhaps the ~ 5 keV curvature observed in ULX, the ~ 0.2 keV soft X-ray excess seen in many AGN, and the ~ 10 keV thermal Comptonization seen in strongly Comptonized VHS of BHB are all physically the same continuum components. There may be an additional hard X-ray (> 10 keV) PL in ULX which would then be analogous to the X-ray PL seen in AGN at $\gtrsim 2$ keV and in VHS of BHBs seen at $\gtrsim 10$ keV. However, at this stage such a component is speculative.

An alternate to the interpretation presented here is that the source harbours a $\sim 10 M_\odot$ black hole with super Eddington accretion (Shakura & Sunyaev 1973; Poutanen et al. 2007; King 2008). For such high accretion rates, the luminosity does not scale with \dot{M} , and instead is given by $L \sim L_{Edd}(1 + \log(\dot{M}/\dot{M}_E))$. Moreover, the characteristic radius at which the luminosity is released is $\sim (27/4)(\dot{M}/\dot{M}_E)r_s$, which is much larger than the standard value of $\sim 5r_s$. The luminosity is also expected to be further enhanced by some moderate beaming. Such an interpretation is attractive because (a) it does not require exotic formation and accretion mechanism needed to explain intermediate mass black holes, (b) the high accretion rates required are perhaps expected when there is thermal time scale mass transfer from donor stars and (c) it explains naturally why the spectra of ULX are distinct from Galactic sources and AGN which are sub-Eddington sources. However, the absence of a simple representation of the expected model spectrum does not allow for detailed spectral analysis. King (2009) associate the soft excess seen in some ULX as emission from such a super Eddington disc. This is reasonable if the soft excess is the energetically dominant component and not for cases like the low flux state of NGC 1313 X-1, where the soft component is less luminous than the main Comptonization one. Another issue is the factor of ~ 2 luminosity variability between the low and high flux states of NGC 1313 X-1. Since luminosity varies as $\log(\dot{M}/\dot{M}_E)$ this would imply a large accretion rate variation which in turn would imply a large variation in the characteristic radius $\propto \dot{M}$. Such a large variation in radius would result in a significant change in the characteristic temperature of the disc, which is not observed. King (2009) invoke variations in the moderate beaming factor to explain such observed variations, which although plausible is rather ad hoc. Finally, if the super Eddington accretion model is correct, then the self consistent standard disc modelling which explains both the spectra as well as the variability versus energy, has to be considered as a coincidence. What is required is a better theoretical prediction of the super Eddington disc spectra which may have to include the possibility of a additional dominant Comptonization component.

In the standard disc framework, there is also a need for better theoretical understanding of a radiation pressure dominated corona as well as a hot inner region. The dynamics of such structures needs to be studied and ascertained that they are viable stable systems. Perhaps more importantly, the results presented in this work need to be confirmed by longer observations of the same source as well as other sources which show similar characteristics. The latter is important since there may be different kinds of ULX, even among the brightest ones.

ACKNOWLEDGMENTS

We thank an anonymous referee for comments/suggestions that improved the presentation of this paper. This work is based on observations obtained with *XMM-Newton*, an ESA science mission with instruments and contributions directly funded by ESA Member States and the USA (NASA). This research has made use of data obtained through the High Energy Astrophysics Science Archive Research Center Online Service, provided by the NASA/Goddard Space Flight Center. The long 123 ks observation was supported by the NASA grant NNX07AE99G. We thank Andrez Zdziarski for helpful discussions.

REFERENCES

- Agrawal V. K., Misra R., 2006, *ApJL*, 638, L83
 Begelman M. C., 2002, *ApJL*, 568, L97
 Colbert E. J. M., Miller M. C., 2005, in Novello M., Perez Bergliaffa S., Ruffini R., eds, *The Tenth Marcel Grossmann Meeting. On recent developments in theoretical and experimental general relativity, gravitation and relativistic field theories* Observational Evidence for Intermediate-Mass Black Holes in Ultra-Luminous X-Ray Sources. pp 530–+
 Devi A. S., Misra R., Agrawal V. K., Singh K. Y., 2007, *ApJ*, 664, 458
 Dewangan G. C., Griffiths R. E., Dasgupta S., Rao A. R., 2007, *ApJ*, 671, 1284
 Dewangan G. C., Griffiths R. E., Rao A. R., 2006, *ApJL*, 641, L125
 Dewangan G. C., Miyaji T., Griffiths R. E., Lehmann I., 2004, *ApJL*, 608, L57
 Dewangan G. C., Titarchuk L., Griffiths R. E., 2006, *ApJL*, 637, L21
 Done C., Kubota A., 2006, *MNRAS*, 371, 1216
 Fabbiano G., Zezas A., King A. R., Ponman T. J., Rots A., Schweizer F., 2003, *ApJL*, 584, L5
 Feng H., Kaaret P., 2005, *ApJ*, 633, 1052
 Feng H., Kaaret P., 2006, *ApJL*, 650, L75
 Feng H., Kaaret P., 2007, *ApJL*, 660, L113
 Feng H., Kaaret P., 2009a, *ArXiv e-prints*
 Feng H., Kaaret P., 2009b, *ApJ*, 696, 1712
 Fridriksson J. K., Homan J., Lewin W. H. G., Kong A. K. H., Pooley D., 2008, *ApJS*, 177, 465
 Gierliński M., Zdziarski A. A., 2005, *MNRAS*, 363, 1349
 Gladstone J. C., Roberts T. P., 2009, *MNRAS*, 397, 124
 Gladstone J. C., Roberts T. P., Done C., 2009, *MNRAS*, pp 948–+
 Goad M. R., Roberts T. P., Reeves J. N., Uttley P., 2006, *MNRAS*, 365, 191
 Haardt F., Maraschi L., 1993, *ApJ*, 413, 507
 Heil L. M., Vaughan S., Roberts T. P., 2009, *MNRAS*, 397, 1061
 Kaaret P., Corbel S., Prestwich A. H., Zezas A., 2003, *Science*, 299, 365
 Kaaret P., Feng H., 2007, *ApJ*, 669, 106
 Kaaret P., Simet M. G., Lang C. C., 2006, *ApJ*, 646, 174
 Kajava J. J. E., Poutanen J., 2009, *ArXiv e-prints*
 King A. R., 2008, *MNRAS*, 385, L113
 King A. R., 2009, *MNRAS*, 393, L41
 King A. R., Davies M. B., Ward M. J., Fabbiano G., Elvis M., 2001, *ApJL*, 552, L109
 Kubota A., Mizuno T., Makishima K., Fukazawa Y., Kotoku J., Ohnishi T., Tashiro M., 2001, *ApJL*, 547, L119
 La Parola V., Peres G., Fabbiano G., Kim D. W., Bocchino F., 2001, *ApJ*, 556, 47
 Liang E. P. T., Price R. H., 1977, *ApJ*, 218, 247
 Magdziarz P., Blaes O. M., Zdziarski A. A., Johnson W. N., Smith D. A., 1998, *MNRAS*, 301, 179
 Méndez B., Davis M., Moustakas J., Newman J., Madore B. F., Freedman W. L., 2002, *AJ*, 124, 213
 Middleton M., Done C., Ward M., Gierliński M., Schurch N., 2009, *MNRAS*, 394, 250
 Miller J. M., Fabbiano G., Miller M. C., Fabian A. C., 2003, *ApJL*, 585, L37
 Miller J. M., Fabian A. C., Miller M. C., 2004, *ApJ*, 607, 931
 Mirabel I. F., Rodríguez L. F., 1999, *ARA&A*, 37, 409
 Miyawaki R., Sugihō M., Kubota A., Makishima K., Namiki M., Tanaka T., Tsunoda N., 2006, in Wilson A., ed., *The X-ray Universe 2005* Vol. 604 of ESA Special Publication, *Spectral Study of Ultra-Luminous Compact X-ray Sources with XMM-Newton and Chandra*. pp 433–+
 Mizuno T., et al. 2007, *PASJ*, 59, 257
 Mucciarelli P., Casella P., Belloni T., Zampieri L., Ranalli P., 2006, *MNRAS*, 365, 1123
 Nowak M., 2005, *Ap&SS*, 300, 159
 Poutanen J., Lipunova G., Fabrika S., Butkevich A. G., Abolmasov P., 2007, *MNRAS*, 377, 1187
 Roberts T. P., 2007, *Ap&SS*, 311, 203
 Shakura N. I., Sunyaev R. A., 1973, *A&A*, 24, 337
 Shapiro S. L., Lightman A. P., Eardley D. M., 1976, *ApJ*, 204, 187
 Stobbart A.-M., Roberts T. P., Wilms J., 2006, *MNRAS*, 368, 397
 Strohmayer T. E., Mushotzky R. F., 2003, *ApJL*, 586, L61
 Strohmayer T. E., Mushotzky R. F., Winter L., Soria R., Uttley P., Cropper M., 2007, *ApJ*, 660, 580
 Strüder L., et al. 2001, *A&A*, 365, L18
 Sugihō M., Kotoku J., Makishima K., Kubota A., Mizuno T., Fukazawa Y., Tashiro M., 2001, *ApJL*, 561, L73
 Sunyaev R. A., Titarchuk L. G., 1980, *A&A*, 86, 121
 Svensson R., Zdziarski A. A., 1994, *ApJ*, 436, 599
 Turner M. J. L., et al. 2001, *A&A*, 365, L27
 Vaughan S., Edelson R., Warwick R. S., Uttley P., 2003, *MNRAS*, 345, 1271
 Winter L. M., Mushotzky R. F., Reynolds C. S., 2006, *ApJ*, 649, 730

- Zdziarski A. A., Gierliński M., 2004, Progress of Theoretical Physics Supplement, 155, 99
Zdziarski A. A., Johnson W. N., Magdziarz P., 1996, MNRAS, 283, 193
Życki P. T., Done C., Smith D. A., 1999, MNRAS, 309, 561